Velocity Estimation and Control of 3-DOF Lab Helicopter Based on Optical Flow

ZHANG Lianhua [1,2]
1. Department of Automation, TNList
Tsinghua University
2. China Astronaut Research and Training Center
Beijing, P.R. China
zhanglh09@mails.tsinghua.edu.cn

LIU Hao , SHI Zongying, ZHONG YiSheng
Department of Automation, TNList
Tsinghua University
Beijing, P.R. China

***Abstract*—This paper presents an angular velocity estimation method based on optical flow to address the hovering and angle tracking control problem for a three degree-of-freedom (3-DOF) lab helicopter. An analytical expression of the travel angular velocity is deduced based on optical flow. Then, a controller consisting of a feedforward controller and a linear quadratic regulation (LQR) state feedback controller is designed. Experiment results on the lab helicopter demonstrate the validity of the angular velocity estimation method and the LQR control strategy.**

Keywords—Optical flow, Vision-based Control, LQR Control, 3-DOF Helicopter

I. INTRODUCTION

In the last two decades, a growing interest has been attracted to the unmanned aerial vehicles (UAVs). The UAVs can carry out various military and civil tasks such as fly reconnaissance, emergency rescue, regular inspection of power lines, etc [1]. UAVs usually rely on the inertial measure unit (IMU) and the global positioning system (GPS) to provide the pose or velocity information. However, in urban and indoor environments, the GPS information may be unreliable or unavailable. Meanwhile, visual sensors are lightweight, cheap and passive, and can provide abundant information about the UAVs' motion and surrounding structure. Consequently, the vision based control, referring to the use of visual data in the closed-loop system to control the motion of a UAV, has gained a growing interest for autonomous flights of aerial vehicles in recent years [2-6].

Vision based control is related to techniques including image processing, state estimation, and controller design. There are many kinds of approaches for state estimation from the visual data, such as target-based pose estimation approach, structure from motion (SFM) scheme, and optical-flow-based estimation method [7]. Target based pose estimation is generally to detect a specific target and to estimate its pose relative to the aerial vehicle. This method requires the target to be kept in the camera field of view and has been widely used for automatic landing and target tracking. The SFM method, as the traditional motion estimation approach, recovers both the camera ego-motion and scene structure by tracking stationary features in the surrounding environment. Therefore, the SFM approach often results in heavy computational burden and large time delay which can hardly meet the control demand of UAV. In recent few years, referring to the behavior of flying insects, some studies using the optical flow method for obstacle avoidance in aerial robotics were carried out as shown in [8-11]. Since optical flow offers relative velocity and proximity information regard to the environment, estimation information from the optical flow was exploited by different control methods for achieving various tasks such as hovering, landing, terrain following, and trajectory tracking [12-16].Optical-flow-based estimation method has the characteristics of less computation, weak dependence on image quality and texture. As an extension of the prior researches as shown in [13-15], an optical flow based controller for hovering and landing on a moving platform was designed using additional information provided by the IMU [12]. However, these control methods based on the average optical flow are complex and not universal [12-15]. In [16], a computational framework based on the nested Kalman filter was proposed and a real-time optic flow-based algorithm for estimating aircraft self-motion and depth map is developed. In the work, the computational burden of filter algorithm was heavy. In [17], a self-motion estimation method from optical flow was proposed based on the continuous homograph constrain and an algorithm for the closed-loop control of a quadrotor was implemented by means of a single camera for the velocity estimation. However, most existing works regulated the linear velocity or height by combining the optical flow with the angular rate information from IMU. There are limited results to estimate angular rate directly from the optical flow.

Based on the optical flow, this paper presents an angular velocity estimation method to deal with the hovering and angle tracking control problem for a three degree-of-freedom (3-DOF) lab helicopter. While the camera is attached to the body of helicopter, the optical flow can be expressed in terms of image coordinates, the linear and angular velocities of helicopter, and

This work is supported by National Natural Science Foundation (NNSF) of China under Grant 61203071 and 61174067.

978-1-4673-5769-2/13/$31.00 ©2013 IEEE

the depth information. Then, an analytical expression of travel angular velocity of the 3-DOF helicopter is deduced based on optical flow. Using the visual feedback, a linear quadratic regulation (LQR) controller is designed for hovering and trajectory tracking, which consists of a feedforward controller and a LQR state feedback controller. Closed-loop experimental results on the lab helicopter demonstrate the effectiveness of the designed estimation and control method.

The remainder of this paper is organized as follows. In Section 2, the self-motion estimation from optical flow is derived. The mathematic model of 3-DOF helicopter is described and an LQR controller is designed in Section 3. Section 4 gives the experimental results obtained on the 3-DOF helicopter. Conclusions are drawn in Section 5.

II. SELF-MOTION ESTIMATION FROM OPTICAL FLOW

Optical flow refers to the apparent velocities of brightness patterns in an image [18]. Let $E(x,y,t)$ denote the image brightness at the point $(x,y)^T$ in the image plane at time t and $(u,v)^T$ represent the optical flow of the point, the optical flow constraint equation can be expressed as follows

$$E_x u + E_y v + E_t = 0,$$

where E_x, E_y and E_t denote the partial derivatives of image brightness with respect to x, y, and t respectively.

Based on the constraint equation, many methods for computing optical flow have been proposed, including differential methods, region-based matching, phase-based, and energy-based techniques. Self-motion estimation from optical flow is to determine the motion of the camera from the sequence of images, under the assumption that optical flow is known at each point in the image. The problem of the self-motion estimation from optical flow was addressed in the field of computer vision [19, 20]. While the camera is attached to the body of the UAV, extracting the motion from image sequences may enable the UAV to perform missions autonomously. In this section, the relation between optical flow and the motion of the UAV is derived from basic transformation between the image coordinate and the world coordinate. Then the angular velocity of a 3-DOF helicopter is deduced.

A. Kinematics of an image point under central projection

We attach a camera to UAV's body and assume that the camera coordinate frame coincides with the body-fixed coordinate frame of the UAV. Then, two reference frames are used to describe the motion of the UAV: the world coordinate frame W and the camera coordinate frame C, which are related via a rotation R and a translation t (see Fig.1) [21]. The rotation matrix $R \in SO(3)$ denotes the rotation from W to C. Let $t_w \in W$ and $t_c \in C$ denote the coordinates of the camera center in the world frame and the world frame's origin in the camera frame respectively. The linear and angular velocities of the camera are given by V and $\Omega \in C$ respectively.

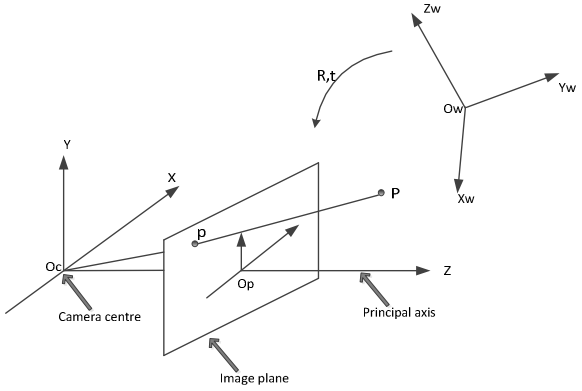

Fig. 1. The relation between the camera and the world coordinate frames.

Let $P_w = (X_w \quad Y_w \quad Z_w)^T \in W$ and $P_c = (X_c \quad Y_c \quad Z_c)^T \in C$ represent a point P in the world frame and the camera frame respectively. Under the pinhole camera model, the point $P \in \Re^3$ in space is projected to the point $p = (x \quad y)^T$ on the image plane, and f represents the focal length of the camera (see Fig.1). Then, the following equations can be obtained

$$P_w = R^T P_c + t_w, \tag{1}$$

$$\dot{R}^T = R^T \Omega_\times, \tag{2}$$

$$V = R\dot{t}_w, \tag{3}$$

$$t_w = -R^T t_c, \tag{4}$$

where the matrix $\Omega_\times$ denotes the skew-symmetric matrix associated with the vector product $\Omega_\times x = \Omega \times x$ for any $x \in \Re^3$.

The central projection from world to the image plane can be expressed in homogeneous coordinates as

$$\begin{pmatrix} x \\ y \\ 1 \end{pmatrix} = \frac{1}{Z_c} \begin{bmatrix} f & 0 & 0 & 0 \\ 0 & f & 0 & 0 \\ 0 & 0 & 1 & 0 \end{bmatrix} \begin{bmatrix} X_c \\ Y_c \\ Z_c \\ 1 \end{bmatrix} = \begin{bmatrix} f & 0 & 0 \\ 0 & f & 0 \\ 0 & 0 & 1 \end{bmatrix} \frac{P_c}{Z_c}. \tag{5}$$

Differentiating both sides of (1) and combining it with (2), one has that

$$\dot{P}_c = -\Omega_\times P_c + R(\dot{P}_w - \dot{t}_w). \tag{6}$$

If the point P is stationary in the world frame, then

$$\dot{P}_w = 0. \tag{7}$$

Substituting (3) and (7) into the (6) results in that

$$\dot{P}_c = -\Omega_\times P_c - V. \tag{8}$$

Taking the derivation of equation (5), one has that

$$\dot{p} = \begin{bmatrix} f & 0 & -x \\ 0 & f & -y \end{bmatrix} \frac{\dot{P}_c}{Z_c}. \tag{9}$$

From (8) and (9), the optical flow can be expressed in terms of image coordinates $(x \quad y)$, the linear and angular velocities of the camera, and the depth Z_c as

$$\dot{p} = \begin{bmatrix} f & 0 & -x \\ 0 & f & -y \end{bmatrix} (-\Omega_\times P_c - V) / Z_c. \tag{10}$$

B. Angular Velocity Estimation of the 3-DOF Helicopter

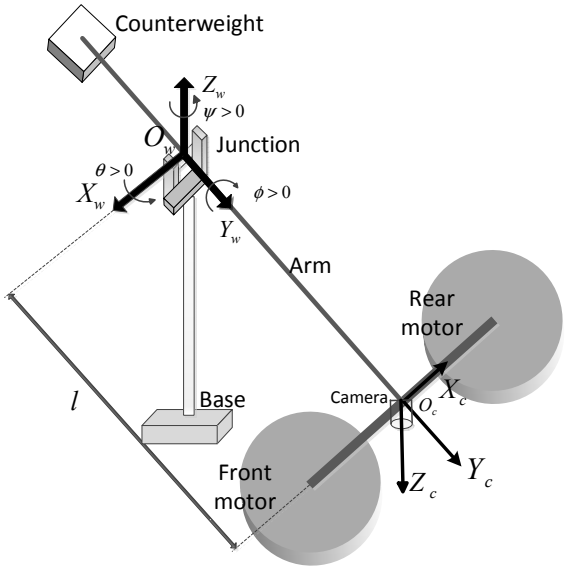

Fig. 2. Schematic of the 3-DOF lab helicopter.

The diagram of the 3-DOF helicopter with a downward-looking camera is illustrated in Fig. 2. Assuming the target point observed by the camera is stationary in the world frame, the following equations can be obtained.

$$t_c = (0, -l, 0)^T, \tag{11}$$

$$\dot{t}_c = 0, \tag{12}$$

where l denotes the distance between the travel axis to the camera placement.

By differentiating (4), one has

$$\dot{t}_w = -R^T (\Omega_\times t_c + \dot{t}_c). \tag{13}$$

Substituting (13) into (6), one can obtain that

$$\dot{P}_c = -\Omega_\times P_c + R\dot{P}_w + \Omega_\times t_c + \dot{t}_c. \tag{14}$$

From (12) and (14), one has that

$$\dot{P}_c = -\Omega_\times P_c + \Omega_\times t_c. \tag{15}$$

Then, substituting (15) into (9), one can obtain that

$$\dot{p} = -\begin{bmatrix} f & 0 & -x \\ 0 & f & -y \end{bmatrix} \Omega_\times \left(\begin{pmatrix} x/f \\ y/f \\ 1 \end{pmatrix} - \frac{t_c}{Z_c} \right). \tag{16}$$

According to the above expression, the motion of the 3-DOF helicopter can be solved by the kinematics of the image of the target points which are stationary in the world frame.

Assume that the elevation angular rate of the helicopter is controlled to attenuate to zero degree. To avoid the effect on the camera optical axis by the pitch motion, the camera is set specially on the arm of the 3-DOF helicopter. Therefore, the depths of different target points are identical to be considered as a constant value z and the angular velocity can be denoted as $\Omega = (0, 0, \omega_z)^T$. Therefore, (16) can be rewritten as

$$\dot{p} = \begin{pmatrix} \dot{x} \\ \dot{y} \end{pmatrix} = \begin{pmatrix} \omega_z (y + f \cdot l / z) \\ -\omega_z \cdot x \end{pmatrix}. \tag{17}$$

Since the optical flow is computed using the position in pixels, we denote $(x_p, y_p)^T$ as pixel coordinates in image and $(u_p, v_p)^T$ the optical flow of the point. Then, (17) can be rewritten in pixel coordinates as

$$\begin{aligned} \begin{pmatrix} u_p \\ v_p \end{pmatrix} &= \begin{pmatrix} \dot{x}_p \\ \dot{y}_p \end{pmatrix} \\ &= \begin{pmatrix} \omega_z [f_x / f_y (y_p - y_0) + f_x \cdot l / z] \\ -\omega_z \cdot f_x / f_y (x_p - x_0) \end{pmatrix}, \end{aligned} \tag{18}$$

where f_x and f_y represent the focal length of the camera in pixels along horizontal and vertical axes respectively. Similarly, (x_0, y_0) are the coordinates of the principal point in pixels. These parameters are called intrinsic parameter of the camera and can be obtained by calibration.

Finally, the travel angular rate can be analytically expressed as

$$\omega_z = \frac{u_p}{f_x / f_y (y_p - y_0) + f_x \cdot l / z}. \tag{19}$$

III. Helicopter Model and Controller Design

As depicted in Fig. 2, two DC motors named front motor and back motor are paralleled implemented in a framework to create thrust forces. As the figure depicts, this helicopter has three degrees of freedom: it can pitch around the long arm, elevate around elevation axis, and travel around the base. Three encoders are connected to this helicopter for measuring the pitch angle $\phi(t)$, elevation angle $\theta(t)$, and travel angle $\psi(t)$. A downward-looking camera is mounted on the long arm to estimate the travel angular rate and travel angle in this experiment.

The dynamic features of 3-DOF lab helicopter plant can be modeled as three freedom rotation which can be described as three second order differential equations by applying the Euler-Lagrange formula respectively [22,23]. After linearization, the dynamical models of three angles can be rewritten as the following forms respectively:

$$\ddot{\theta}(t) = a_1\dot{\theta}(t) + a_2\theta(t) + a_3u_\theta(t) + a_4, \quad (20)$$

$$\ddot{\phi}(t) = b_1\dot{\phi}(t) + b_2\phi(t) + b_3u_\phi(t), \quad (21)$$

$$\ddot{\psi}(t) = c_1\dot{\psi}(t) + c_2\psi(t) + c_3\phi(t), \quad (22)$$

where $u_\theta(t)$ and $u_\phi(t)$ are the control inputs, which means the sum value and the difference value of the applied voltages on the front and back motors. a_i $(i = 1, 2, 3, 4)$, b_i $(i = 1, 2, 3)$, and c_i $(i = 1, 2, 3)$ are helicopter parameters.

Let

$$X_\theta(t) = \left[x_{1\theta}(t) \quad x_{2\theta}(t) \quad x_{3\theta}(t)\right]^T,$$

where $x_{1\theta}(t) = \theta(t) - \theta_r(t)$, $\theta_r(t)$ is the desired elevation angle, $x_{2\theta}(t) = \dot{x}_{1\theta}(t)$, and $\dot{x}_{3\theta}(t) = x_{1\theta}(t)$. Then, the state-space model of the elevation channel can be described by the following equation as

$$\dot{X}_\theta(t) = A_\theta X_\theta(t) + B_\theta\left[a_3u_1(t) + z_{r\theta}\right], \quad (23)$$

where

$$A_\theta = \begin{bmatrix} 0 & 1 & 0 \\ a_2 & a_1 & 0 \\ 1 & 0 & 0 \end{bmatrix}, \; B_\theta = \begin{bmatrix} 0 \\ 1 \\ 0 \end{bmatrix},$$

and $z_{r\theta} = -\ddot{\theta}_r(t) + a_1\dot{\theta}_r(t) + a_2\theta_r(t) + a_4$.

Besides, let

$$X_\psi(t) = \left[x_{1\psi}(t) \quad x_{2\psi}(t) \quad x_{3\psi}(t) \quad x_{4\psi}(t) \quad x_{5\psi}(t)\right]^T,$$

where $x_{1\psi}(t) = \psi(t) - \psi_r(t)$, $\psi_r(t)$ is the desired travel angle, $x_{2\psi}(t) = \dot{x}_{1\psi}(t)$, $x_{3\psi}(t) = \phi(t) + (c_1\dot{\psi}_r + c_2\psi_r - \ddot{\psi}_r)/c_3$, $x_{4\psi}(t) = \dot{x}_{3\psi}(t)$ and $\dot{x}_{5\psi}(t) = x_{1\psi}(t)$.

From (21) and (22), the state-space model of the travel channel can be obtained as follows

$$\dot{X}_\psi(t) = A_\psi X_\psi(t) + B_\psi\left[b_3u_\phi + z_{r\psi}\right], \quad (24)$$

where

$$A_\psi = \begin{bmatrix} 0 & 1 & 0 & 0 & 0 \\ c_2 & c_1 & c_3 & 0 & 0 \\ 0 & 0 & 0 & 1 & 0 \\ 0 & 0 & b_2 & b_1 & 0 \\ 1 & 0 & 0 & 0 & 0 \end{bmatrix}, \; B_\psi = \begin{bmatrix} 0 \\ 0 \\ 0 \\ 1 \\ 0 \end{bmatrix},$$

and

$$z_{r\psi} = [-\dddot{\psi}_r + (b_1 + c_1)\ddot{\psi}_r + (b_2 + c_2 - b_1c_1)\dot{\psi}_r - (b_1c_2 + b_2c_1)\dot{\psi}_r - b_2c_2\psi_r]/c_3.$$

The controller is constructed by two parts: a feedforward controller and a LQR controller; that is, the control inputs have the following indexes

$$u_i(t) = u_i^{FF}(t) + u_i^{LQR}(t), \; i = \theta, \; \psi, \quad (25)$$

where $u_i^{FF}(t)$ $(i = \theta, \; \psi)$ are the feedforward control inputs and are given by

$$u_\theta^{FF}(t) = -\frac{z_{r\theta}}{a_3}, \quad (26)$$

and

$$u_\psi^{FF}(t) = -\frac{z_{r\psi}}{b_3}. \quad (27)$$

The LQR control inputs $u_i^{LQR}(t)$ are designed for the following error systems

$$\dot{X}_i = A_iX_i(t) + B_iu_i^{LQR}(t), \; i = \theta, \; \psi,$$

for the performance forms

$$J = \int_0^\infty \left[X_i^T(t)Q_iX_i(t) + r_i(u_i^{LQR}(t))^2\right]dt, \; i = \theta, \; \psi \quad (28)$$

where Q_i is a positive definite matrix and r_i is a positive constant.

Let

$$u_\theta^{LQR}(t) = -\frac{1}{a_3}K_\theta X_\theta(t), \quad (29)$$

and

$$u_\psi^{LQR}(t) = -\frac{1}{b_3}K_\psi X_\psi(t), \quad (30)$$

where K_i $(i = \theta, \; \psi)$ are the solutions to the above LQR problem. K_i $(i = \theta, \; \psi)$ can be obtained by

$$K_i = r_i^{-1}B_i^TP_i, \; i = \theta, \; \psi,$$

where P_i $(i = \theta, \; \psi)$ is the positive definite solution of the following associated Riccati equations

$$A_i^TP_i + P_iA_i - r_i^{-1}P_iB_iB_i^TP_i + Q_i = 0, \; i = \theta, \; \psi.$$

The configuration of the whole control system is depicted in Fig. 3. Although the elevation angle and the travel angle are controlled by the same control method, the control periods are required differently for different channels. In fact, the elevation angle and the pitch angle determine the attitude of the helicopter, and their control periods should be as short as possible to ensure the stability. From (24) we know that the control of pith angle can be seen as the inner-loop for controlling the travel angle. Travel angle determines the position of the helicopter, and whose sampling rate can be relatively low. In the closed-loop system, visual feedback is used to control the travel angle.

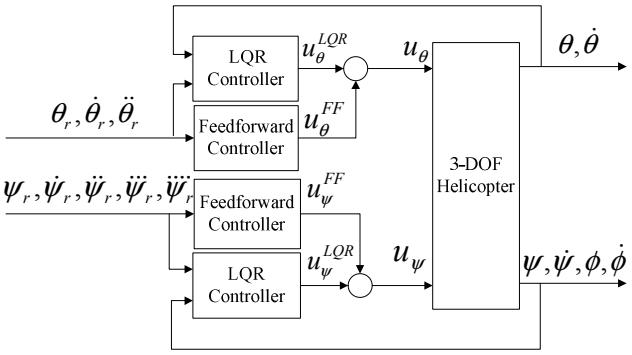

Fig. 3. The configuration of the LQR control system.

IV. EXPERIMENTAL RESULTS

As shown in fig.4, the experimental system consists of seven parts: a 3-DOF laboratory helicopter, which is produced by the Quanser Company [24], three encoders, a USB camera fixed on the arm of the helicopter, a laptop which acquires the video from the camera and runs the optical flow computation and angular velocity estimation algorithms, a dSPACE system, a personal computer (PC), and two power amplifiers. The elevation, pitch and travel angles are measured by three encoders and transmitted to the dSPACE. The travel encoder has an effective resolution of 0.0439 deg and the travel angle measured by encoder is used as the ground truth to compare with the travel angular data from optical flow in the experiment. The sampling rate of the USB camera is 60Hz and resolution is 160*120 .

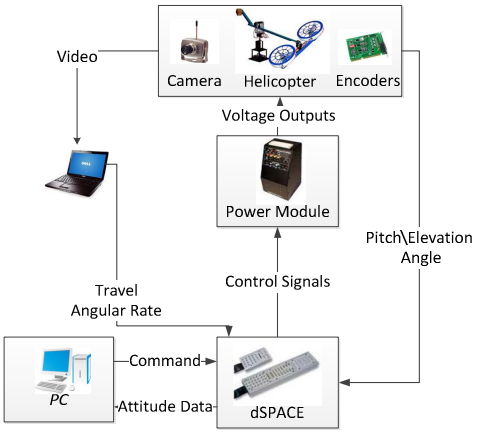

Fig. 4. Schematic of the experimental setup.

The indoor floor is used as the target plane with poor texture. Before the experiment beginning, the calibration of the camera has been done by using the Camera Calibration Toolbox for Matlab. A Pyramidal implementation of the Lukas-Kanade algorithm [25] provided with OpenCV is used to compute the optical flow. In the visual program, a timer with 60Hz frequency is set to capture the image, compute the optical flow, and estimate the angular rate. Then, the travel angular rate based on vision was transmitted to dSPACE by RS422 and filtered with a low-pass filter. The travel angle is acquired by the integral of the filtered travel angular rate.

In our experiments, the elevation angular rate of the helicopter is controlled to zero degree so that the depth is a constant value. Three different experiments are conducted to check the effectiveness of the angular velocity estimation and LQR method on the 3-DOF helicopter.

Case1: A manual test is carried out to test the validity of the travel angular rate based on vision and compute the proportion coefficient between the ground truth and the vision based travel angle rate.

In this case, the travel angular rate varies by manual operation within [−1,1] rad/s, whereas the elevation and pitch angles keep at 0 deg. Both the filtered and unfiltered outputs based on optical flow are presented to compare with the ground truth in Fig. 5. From this figure, one can see that the visual travel angle rate fit well with the ground truth from the encoder. It is shown that the angular velocity estimation algorithm is valid and the noises were effectively filtered by the low-pass filter. From Fig. 5, one can estimate the lag introduced by the visual processing and filtering to approximate 200 ms.

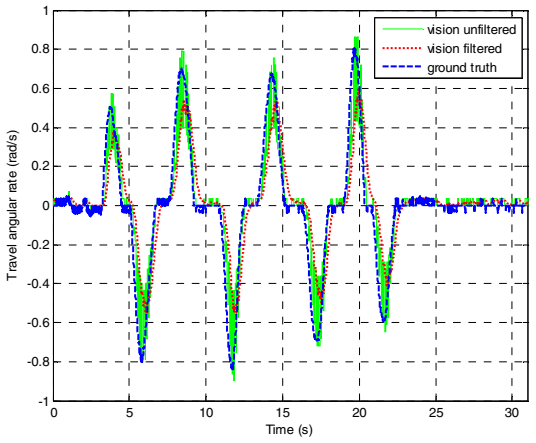

Fig. 5. Manual test results.

Case 2: The 3-DOF helicopter is controlled to carry out hovering task while the elevation and travel angles are stabilized at 0 deg by the LQR controller.

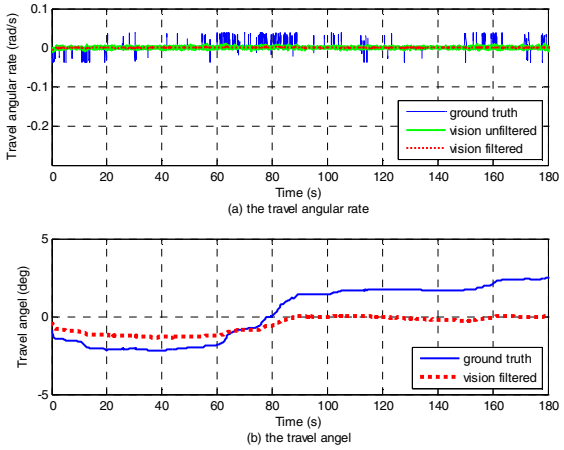

Fig. 6. Hovering mission.

In the experiment, the visual travel angular rate and travel angle obtained by integrating are introduced as feedbacks of the LQR controller instead of travel angle from encoder. Corresponding responses are described in Fig. 6. From this figure, one can see that both the filtered and unfiltered visual travel angular rate approximate zero and the angular rate of ground truth is less than ±0.1 rad/s in the steady-state. Besides, the steady-state error of the visual travel angle is less than

±0.3 deg. In addition, along with the growth of the integration time, the integral drift of travel angle increases in comparison with the ground truth. One can see that the closed-loop system achieves good steady-state performance.

Case 3: The step response performance of the closed-loop system for the travel channel is evaluated.

The desired reference signal is generated by $\psi_r = \lambda_\psi w_\psi / (s + \lambda_\psi)$, where ψ_r is the travel angle reference signal, w_ψ are the step waveform signal with amplitude of 10 deg. Corresponding response for travel channel is presented in Fig. 7. From this figure, one can see that the settling time with 5% criterion for travel angle is 16 s and the steady-state error is less than 0.5 degree. It shows that good dynamical tracking performance is achieved for the travel angle with the visual feedback.

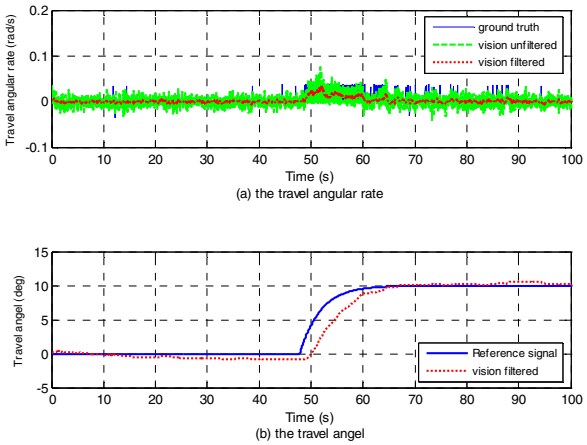

Fig. 7. Step response of the travel angle.

V. CONCLUSIONS

In this paper, an optical flow-based angular velocity estimation method was proposed for the 3-DOF helicopter. Based on the LQR control method, closed-loop control of the 3-DOF helicopter is achieved. Experiment results on the 3-DOF helicopter demonstrated the validity and efficiency of the angular velocity estimation method in spite of low resolution image and poor texture, which result in noisy optic flow estimation. Furthermore, closed-loop system also achieves good steady-state performance and dynamical tracking performance by the designed LQR controller.

REFERENCES

[1] K. P. Valavanis, Advances in unmanned aerial vehicles, Berlin:: Springer, 2007.

[2] F. Chaumette and S. Hutchinson, "Visual servo control. I. Basic approaches," Robotics & Automation Magazine, IEEE, vol. 13, pp. 82--90, 2006.

[3] E. Altug, J. P. Ostrowski and C. J. Taylor, "Control of a quadrotor helicopter using dual camera visual feedback," The International Journal of Robotics Research, vol. 24, pp. 329--341, 2005.

[4] R. Mahony, P. Corke and T. Hamel, "Dynamic image-based visual servo control using centroid and optic flow features," Journal of Dynamic Systems, Measurement, and Control, vol. 130, p. 011005, 2008.

[5] L. Mejias, S. Saripalli, P. Campoy, and G. S. Sukhatme, "Visual servoing of an autonomous helicopter in urban areas using feature tracking," Journal of Field Robotics, vol. 23, pp. 185--199, 2006.

[6] H. Romero, S. Salazar and R. Lozano, "Real-time stabilization of an eight-rotor UAV using optical flow," Robotics, IEEE Transactions on, vol. 25, pp. 809--817, 2009.

[7] F. Kendoul, "Survey of advances in guidance, navigation, and control of unmanned rotorcraft systems," Journal of Field Robotics, vol. 29, pp. 315–378, 2012.

[8] J. C. Zufferey and D. Floreano, "Fly-inspired visual steering of an ultralight indoor aircraft," Robotics, IEEE Transactions on, vol. 22, pp. 137--146, 2006.

[9] A. Beyeler, J. C. Zufferey and D. Floreano, "Vision-based control of near-obstacle flight," Autonomous robots, vol. 27, pp. 201--219, 2009.

[10] J. S. Humbert, A. Hyslop and M. Chinn, "Experimental validation of wide-field integration methods for autonomous navigation," in Proceedings of the IEEE/RSJ International Conference on Intelligent Robots and Systems, 2007, pp. 2144--2149.

[11] J. Conroy, G. Gremillion, B. Ranganathan, and J. S. Humbert, "Implementation of wide-field integration of optic flow for autonomous quadrotor navigation," Autonomous robots, vol. 27, pp. 189--198, 2009.

[12] B. H E Riss E, T. Hamel, R. Mahony, and F. X. Russotto, "Landing a vtol unmanned aerial vehicle on a moving platform using optical flow," Robotics, IEEE Transactions on, vol. 28, pp. 77--89, 2012.

[13] B. Herisse, T. Hamel, R. Mahony, and F. X. Russotto, "A terrain-following control approach for a VTOL Unmanned Aerial Vehicle using average optical flow," Autonomous Robots, vol. 29, pp. 381--399, 2010.

[14] B. Herisse, F. X. Russotto, T. Hamel, and R. Mahony, "Hovering flight and vertical landing control of a VTOL unmanned aerial vehicle using optical flow," in Proceedings of IEEE International Conference on Intelligent Robots and System, 2008, pp. 801--806.

[15] B. Herisse, T. Hamel, R. Mahony, and F. X. Russotto, "A nonlinear terrain-following controller for a VTOL unmanned aerial vehicle using translational optical flow," in Proceedings of IEEE International Conference on Robotics and Automation, 2009, pp. 3251--3257.

[16] F. Kendoul, I. Fantoni and K. Nonami, "Optic flow-based vision system for autonomous 3D localization and control of small aerial vehicles," Robotics and Autonomous Systems, vol. 57, pp. 591--602, 2009.

[17] V. Grabe, H. H. Bulthoff and P. R. Giordano, "On-board velocity estimation and closed-loop control of a quadrotor UAV based on optical flow," in Proceedings of IEEE International Conference on Robotics and Automation, 2012, pp. 491--497.

[18] B. K. P. Horn and B. G. Schunck, "Determining optical flow," Artificial intelligence, vol. 17, pp. 185--203, 1981.

[19] T. Y. Tian, C. Tomasi and D. J. Heeger, "Comparison of approaches to egomotion computation," , in Proceedings of IEEE Computer Society Conference on Computer Vision and Pattern Recognition, 1996, pp. 315--320.

[20] A. R. Bruss and B. K. P. Horn, "Passive navigation," Computer Vision, Graphics, and Image Processing, vol. 21, pp. 3--20, 1983.

[21] R. Hartley and A. Zisserman, Multiple view geometry in computer vision second edition, U.K: Cambridge Univ Press, 2004.

[22] J. Shan, H. T. Liu and S. Nowotny, "Synchronised trajectory-tracking control of multiple 3-DOF experimental helicopters," IEE proceedings-Control Theory Applications, ,vol152, pp. 683--692. 2005.

[23] H. Liu , G. Lu and Y. S. Zhong, "Robust LQR attitude control of a 3-DOF lab helicopter for aggressive maneuvers", IEEE Trans. on Industrial Electronics, to be published.

[24] "3-DOF helicopter reference manual", The Quanser Consulting Inc., 2006.

[25] B. D. Lucas, T. Kanade and Others, "An iterative image registration technique with an application to stereo vision," in Proceedings of the 7th international joint conference on Artificial intelligence, 1981, pp. 674–679.